An Experimental Study of Turbidite Channel Deposits: Implications for Channel Evolution and Sandstone Deposits

James Buttles
Earth Resources Laboratory
Department of Earth, Atmospheric, and Planetary Sciences
Massachusetts Institute of Technology
Cambridge, MA 02139

Burke Minsley
Schlumberger - Western Geco
Houston, TX

Will Schweller
Chevron Petroleum Technology Corporation
San Ramon, CA 94583

John Grotzinger
Earth Resources Laboratory
Department of Earth, Atmospheric, and Planetary Sciences
Massachusetts Institute of Technology
Cambridge, MA 02139

May 11, 2001

Abstract

Gaining a detailed understanding of turbidite bed sequences is important for the characterization of sandstone reservoir properties, correlation of well cores, and geological interpretation. Many factors influence the internal structure of sandstone reservoirs: source material, source location in time, transport processes, basin geometry, fan channel development and evolution to name a few. Sandstone deposits associated with channel complexes are easy to find but difficult to develop. Here, we conduct tank experiments of scaled sediment-laden turbidity currents traversing a submerged channel to: (1) establish a state-of-the-art data collection and data processing system that has the potential to gain a unique understanding

of the processes and deposits that build submarine fan environments; and (2) to use the facility to demonstrate how the interaction of a depositive turbidity current with a sinuous channel may influence the geometry, spatial relationships and grain size sorting of sandstone deposits. Our data shows the construction of prominent levees, asymmetric levee growth, continuous channel overspill, enhanced channel overspill downstream of bend corners, and lobate-shaped lobe deposits. Our preliminary results are qualitative, but indicate that channel wavelength, bend curvature, and bend peak-to-peak amplitude may have strong controls on down-channel and cross-channel depositional patterns, deposit thickness and grain size sorting.

1 Introduction

Channels on submarine fans transport and distribute sediment on fan surfaces (Normark et al., 1993; Mutti and Normark, 1991). Sediments deposited on submarine fans are primarily of terrestrial origin, containing a portion of organic detritus. Over geologic time this detritus may be transformed into hydrocarbons and migrate to and collect within turbidite sandstone deposits. Submarine channels compose a sub-environment of a fan and are often bounded by levees that are generally asymmetric and decrease in height in the down-channel direction (Manley et al., 1997; Normark et al., 1993). Channels that build submarine fans tend to develop distributaries in the downstream direction, have associated depositional lobes, and periodically avulse. In addition, spatial changes in channel sinuosity, slope, and cross section will affect the dynamics of passing gravity currents. Therefore, deposits and depositional patterns within a channel complex contain a complicated record of the interaction of a gravity current with the channel geometry in space and time. Lateral and vertical bed connectivity and lateral changes in reservoir significant rock properties, such as grain size, will be reflected in the resulting deposits.

In this paper we attempt to accomplish two goals through a series of experiments:

1. Develop an integrated, state-of-the-art data collection and data processing system that has the potential to gain a unique understanding of the processes and deposits that build submarine fan environments.

2. Use the facility to demonstrate how the interaction of a depositive turbidity current with a sinuous channel may influence the geometry, spatial relationships and grain size sorting of sandstone deposits.

2 Experimental Setup and Data Collection

2.1 Apparatus

The experimental apparatus has four primary components: a basin tank, a slurry tank, a clear water tank, and a deposit mapping bridge (Figure 1).

A basin tank 4.58 x 4.58 x 1.2 m (l x w x h) is fitted with a polypropylene false floor with dimensions 4.25 x 4.25 m and a diagonal length of $\sim$ 4.9 m. The smaller false floor introduces a moat which prevents the reflection of a current off the side walls. When a current passes into the moat it is drained away by perforated pipes.

A 50 vol.% slurry is mixed in a tank located $\sim$ 5.0 m above the lab floor (B in Figure 1). The slurry consists of water, fine blown silica (balotini) and ground silica. The sediment is proportioned by 90% balotini and 10% ground silica. The grain size distribution of each sediment component is not known at this time, but the balotini grain size range may be similar to that determined from other studies ($5\mu - 80\mu$). Known sediment characteristics and input volumes are included in Table 1.

Table 1: Experimental Parameters and Channel Geometry

Parameter	Value	Comment
D_b	30	mean grain size (μ) (balotini)
D_{gs}	19	mean grain size (μ) (ground silica)
V_{sb}	8.4	mean size settling velocity (mm/s)
W_b	14.3	balotini mass/expt. (kg)
W_{gs}	1.6	ground silica mass/expt. (kg)
Vol_{H_2O}	8.5	volume H_2O (l)/expt.
W_1/d	8.1	max channel width/channel depth
W_2/d	3.2	min channel width/channel depth
h_c/d_1	0.26	est. current height/max. channel half width
h_c/d_2	0.67	est. current height/min. channel half width
λ/W_1	6.58	wavelength/max. channel width
λ/W_2	16.67	wavelength/min. channel width

When the sediment and water are completely mixed the slurry is released into a feeder pipe connected to the upper tank. The feeder pipe transports the slurry to an outlet pipe (pipe beneath the large tank in Figure 1) which is connected to a clear water tank (volume of 1200 l). The clear water and the slurry mix in the outlet pipe to produce a homogeneous dilute ($2-5\%$ by mass) mixture (Parsons et al., 2001).

As the mixture leaves the outlet pipe it passes into a momentum reduction box. This box removes the excessive amount of forward momentum the mixture gains due to the large flow rate out of the clear water tank. With the forward momentum removed, the incoming jet transforms to a sediment-laden plume driven by buoyancy alone (Parsons et al., 2001). The plume then exits the momentum box and moves out of the source region as a sediment-laden turbidity current. The duration of each experiment is 7-10 minutes.

Finally, a Cartesian grid mapping bridge surrounds the basin tank. The bridge is composed of two tracks, a probe track and a bridge track, with each track moved by an independent servo motor (Figure 1). Motion can be independent (normal x-y mapping) or simultaneous (angular or x′-y′ mapping). Acoustic probes (ultrasonic and ADV) are attached to the probe track via an

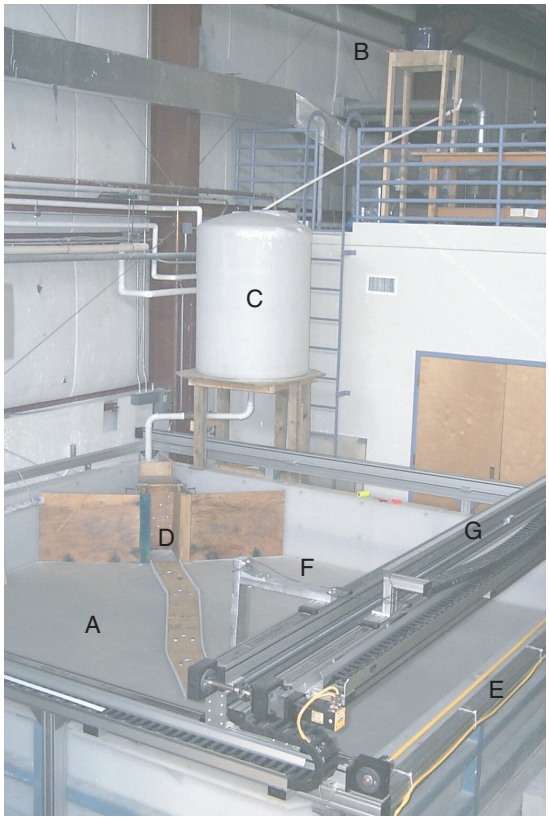

Figure 1: Experimental apparatus. A-basin tank; B-slurry tank; C-clear water tank; D-turbidity current source box; E-mapping bridge supports; F-ultrasonic/ADV probe mount; G-probe/bridge motion tracks.

extension arm. Data collection and mapping system motion are controlled using a standard PC running Windows 95. The two tracks are generally moved by a user written motion control program. The motion control program is also linked (via a hard-wired sinc) to the ultrasonic probe through the user programmable software Labview (see section 2.3 below).

2.2 Channel Construction and Geometry

The experimental channel and associated geometry is shown in Figure 2. Balotini is used as the base sediment for the channel. The channel is constructed by first pouring dry sediment (to a pre-determined depth) into a rectangular box placed on the tank floor. The tank is then slowly filled from the bottom up to a depth just above the rectangular box. The form is allowed to set for one day to ensure the sediment is fully saturated. After this time the surrounding water is drained and the rectangular box is removed. Due to the water saturation, the sediment inherits a bulk strength and maintains its shape. It is this bulk strength that allows the sediment form to be cut into any shape.

A plywood template is cut with the initial geometry and shape of the channel. The plywood template is then lowered onto the surface of the sediment and lightly tapped down. Tapping the template imprints the channel shape on the sediment surface. Sediment is then removed (to a fixed depth) from within the channel imprint. Initially, the banks outside the channel are flat and the channel relief is approximately constant along the channel length. Reducing the bank relief with downstream distance would be more realistic (Normark et al., 1993) and will be addressed in future experiments. The tank is then slowly refilled to the water depth used in an experimental run (relative depth of 60 cm).

The geometric parameters of the channel are included in Table 1. It should be noted in Figure 2 that the sides and edges of the channel do not maintain a vertical profile. Refilling the tank causes the edges to slump to an equilibrium slope imposed by the relative depth or relief of the channel. Due to sediment slumping, the channel width varies with height. The maximum width is $\sim$ 38 cm, and the minimum width is $\sim$ 15 cm.

2.3 Data Collection and Processing

We currently collect turbidite deposit data, bed aggradation rate data and current velocity data for each experimental run. In addition, we extensively section and core the deposit, though we have yet to begin this process by the writing of this paper. The first two data types are collected using an ultrasonic probe and the last type using an acoustic Doppler device. Using the equipment in concert provides state of the art laboratory data collection capabilities.

Three component (x, y, z) mean current velocities are recorded during a run using an Acoustic Doppler Velociometer (ADV). A primary advantage of this device is its non-intrusive character. The sampling volume of the ADV lies well below its transducer arms. ADV data is useful in interpreting the link between the fluid mechanics and turbidity current deposit characteristics. In the

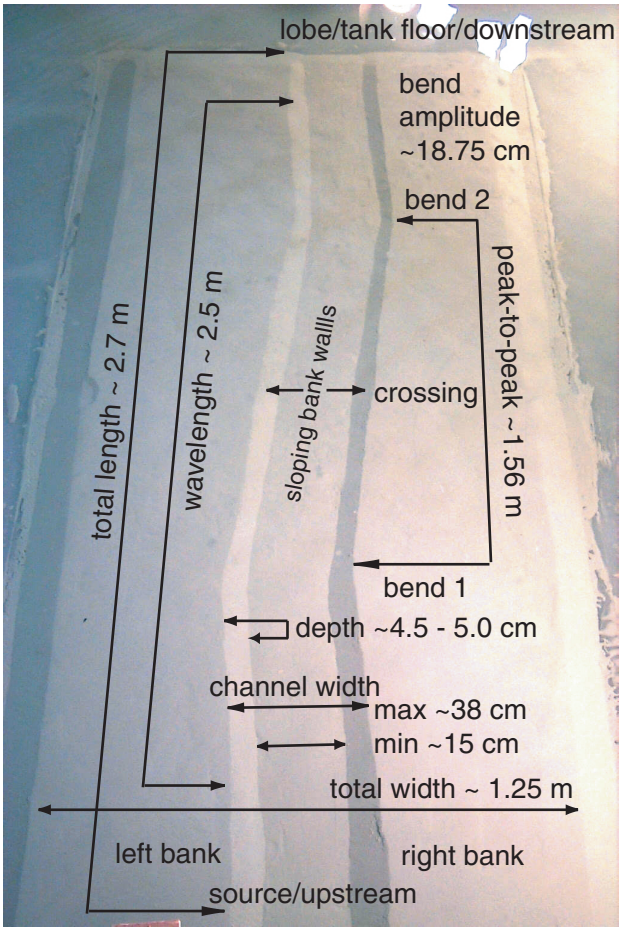

Figure 2: Initial channel geometry.

context of the current experiments, ADV data may be useful for recognition of secondary currents (i.e., cross-stream currents near channel bends) which may be characterized and interpreted in terms of channel geometry and cross-channel sediment deposits and vise versa.

Deposit depths are determined from bed surface reflections of ultrasound energy. Source acoustic energy is generated by an Ultran Laboratories ultrasound transducer (models ws75-1 or ws75-2, 1 MHz or 2 MHz optimal frequency respectively) connected to a JSR Ultrasonics DPR 35+ pulse/reciever. Firing of the transducer (also referred to as the ultrasonic probe or just probe) is controlled through a PC using Labview software via a National Instruments BNC-2110 adapter. The system is currently set up with the transducer acting as source and receiver, but can be reconfigured to accommodate an independent source and independent receiver. Also, the system is set up using only one channel, but can be expanded to include three additional channels.

Turbidite deposit depth and aggradation rates are processed and recorded using Labview software. In general, the collection and processing procedure of the Labview program we have developed (a Labview vi) is to collect raw reflection data from a point (and ultimately a number of points) on the deposit surface and output an averaged reflection trace. In all of the experiments we set the number of traces/point to be averaged to 50. Additional inputs include the average trace sampling window, which changes slightly for each experiment but is generally $100\mu s$, and water velocity model (assumed to be constant with a range of 1440-1460 m/s). The first break of the averaged trace is determined by defining a threshold amplitude value above which the trace amplitude must be. Deposit depth is then calculated using the two-way travel time of the first break pick and the water velocity model. The averaged trace (amplitude time series) and depth are output to the screen and saved as text files. Estimate of the depth resolution is between 300μ and 500μ but may be as low as 100μ.

Data are collected at numerous points on a deposit, taking many hours to complete (17082 points and $\sim$ 14 hrs respectively for each experimental run in the current setup). Collecting and saving this amount of data (180 MB to 2 GB) over this length of time is accomplished by programming Labview to communicate with the bridge motion program through a hard wired sinc (or trigger). The Labview program collects its required traces at a point while the motion control program waits for the trigger from Labview. When the data are collected and saved, the bridge motion program is triggered and the probe and/or bridge moves. This process continues until Labview reaches a prescribed number of points.

Saved depth data are then post processed to correct errors. Two errors dominate our output traces, depths that are too shallow and depths that are too deep (relative to the known maximum and minimum deposit depths). Shallow depth errors are corrected by visually inspecting the depth output data to determine at what depth the error begins. The original depth output file is then resampled through a second Labview program that applies a narrowed sampling window. The proper first break is picked and the correct depth is calculated. Excessive depth errors are corrected using a C program that inputs the newly corrected

depth file. This program picks out the deep depth errors and replaces them with the average of their neighbors. Once this is complete, all of the depth data is smoothed by applying a bi-direction averaging technique. The final product is a corrected and smoothed depth output file (e.g. see Figure 9).

3 Experimental Results

3.1 Turbidity Current Scaling

In the following experiments the height of the body of the current is estimated to be on the order of the channel depth, $h_c \sim 5$ cm, the front velocity estimated at $U_f \sim 10 - 12$ cm/s (determined from videos), and the dimensionless depth $\frac{h_c}{H} \simeq 0.08$ (H is the total fluid depth). Using these values and assuming a bulk suspended sediment concentration of $\sim 2\%$ by mass and a submerged specific gravity of 1.65, a Richardson number of 1.25 is estimated. Therefore, currents in these experiments are slightly subcritical. Also, the magnitudes of h_c and U_f of the current imply Reynolds similarity (Parsons et al., 2001; Garcia and Parsons, 1996). Therefore, frictional effects on the turbulence and the associated sediment deposition should be negligible. However, there is an exception to the last statement which is applicable when a current is confined. Frictional effects may be important if the ratio of the current height to the channel half width ($\frac{h_c}{d_i}$, $d_i = \frac{W_i}{2}$, i = max. or min. channel width) is too large. Generally, to neglect geometrical friction the ratio $\frac{h_c}{d_i} \ll 1$. In the present experiments, $\frac{h_c}{d_i}$ initially ranges from 0.26-0.67 (Table 1). This issue will be addressed in a subsequent section. Finally, it should be noted that the experimental results are applicable to submarine fans which exhibit similar source sediment particle Reynolds numbers.

3.2 Turbidity Currents Traversing a Channel

3.2.1 Current Evolution: From Start to Finish

Figures 3 - 6 show the time sequence of an experimental turbidity current traversing the submerged channel. The duration of the experiment is ∼10 minutes. In Figure 3a the current front is just passing bend 1. The body of the current slightly overspills on both the right and left banks, though the overspill just before the left bank of bend 1 is stronger than that upstream of the bend. Overspill occurs because the current height is on the order of the channel depth, thus diffusion tends to transport sediment from the channel to the surrounding water and bank regions. In Figure 3b the current front has passed bend 1. By this time overspill on the left bank has increased, especially near the left bank of bend 1. In contrast, overspill on the right bank has changed little. In Figure 4a the current front has reached the crossing between bend 1 and bend 2. Left bank overspill continues to increase while the current follows the channel geometry. A change in the character of the left bank overspill can be seen in Figure 4b. As the current front moves into bend 2, left bank overspill near the

current front is substantially reduced along the straight channel section. The left bank overspill region continues to expand, but becomes distinctly associated with the geometry of bend 1. Overspill on the right bank has also increased, though it predominantly occurs before bend 1.

In Figure 5a the current front has passed bend 2. Right bank overspill at bend 2 is similar in character to that at bend 1, but is much less developed. Sediment overspill on the left bank continues to increase. The spreading characteristics of the overspilling sediment is apparent at this time. The sediment spreads laterally or approximately perpendicular to the channel axis upstream of bend 1. Spreading at and beyond bend 1 occurs in a radial pattern extending from the apex of bend 1 along the straight channel segment. This spreading pattern may have implications for the occurrence of sediment waves observed on levee flanks in the submarine environment (McHugh and Ryan, 2000). Although the amount of overspilling sediment appears large, the majority of the sediment is still confined and transported in the channel. This can be determined by observing the lighting contrast between the overbanking and channelized portions of the current.

In Figure 5b the front of the current has passed beyond the channel end. Overspilling sediment on the left bank continues to expand. Sediment overspilled from bend 1 has now reached the left bank of bend 2. Overspill at bend 2 has also increased, but is still not as laterally extensive as that at bend 1. As the front of the current exits the channel, it is no longer confined and therefore begins to spread laterally. The dominant component of motion is still in the downstream direction as can be seen by the cone shape of the expanding front. Figure 6 shows the final deposit at the exit of the channel. The cone shape character of the deposit is apparent. This shape may be the result of prior current confinement, or it may be related to the drop in elevation between the channel exit and the tank floor (channel/floor transition) which is initially on the order of 1 cm.

3.2.2 Current Evolution: Variations Among Experiments

Figure 7 shows the front of the current in the vicinity of bend 1 for experiments 1, 4, 5, and 6. The amount of overspill on both banks substantially increases as the channel depth decreases. As the channel aggrades, lower layers of the current move closer to the tops of the channel banks. For similar input conditions, more of the current is above the channel banks. This promotes increased amounts of overspill. Again, even though the amount of overspilling sediment increases as the channel aggrades, the majority of sediment is still confined and transported within the channel banks.

Currents in later experiments expand as a wedge of fluid with their widest cross section near the source (e.g. Figure 7, Expt. 4). Expansion of the current in this manner is similar to that proposed by Peakall et al. (2000). In general, the current is less influenced by the channel geometry upstream of bend 1. Sediment overspilling in this region spreads out radially.

Figure 8 shows a comparison of overspilling between experiment 1 and exper-

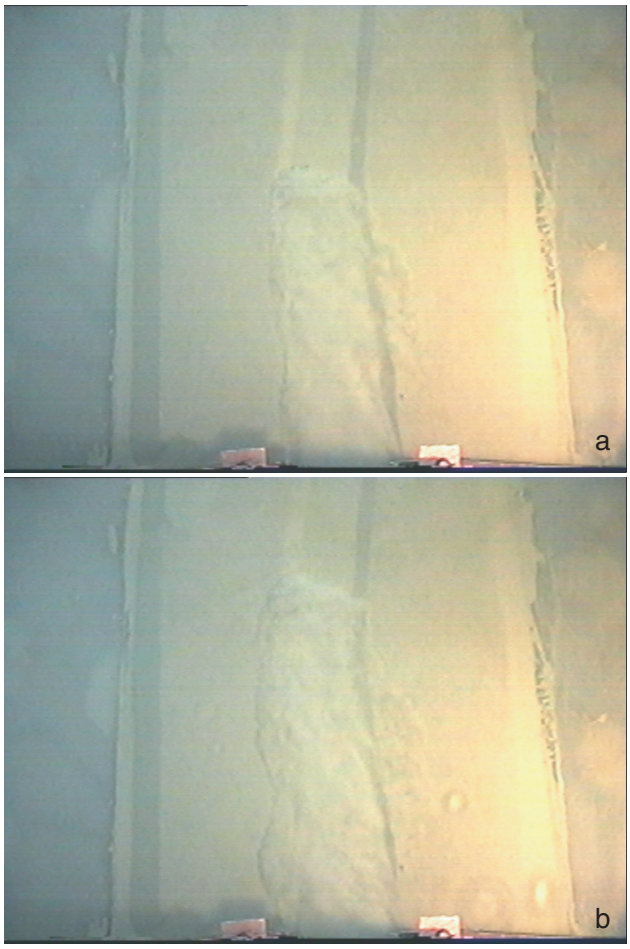

Figure 3: Experimental turbidity current traversing the channel.

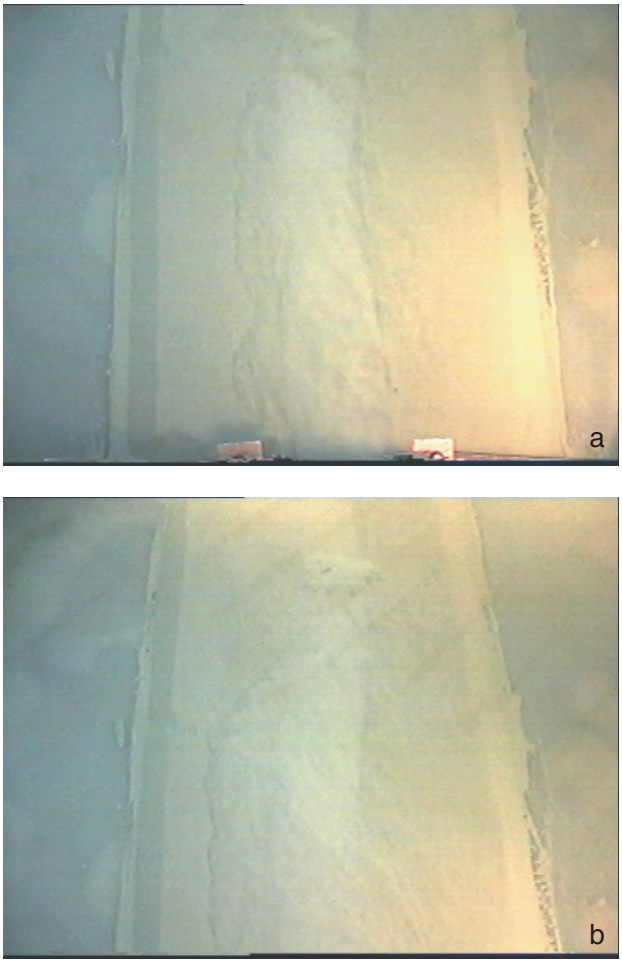

Figure 4: Experimental turbidity current traversing the channel.

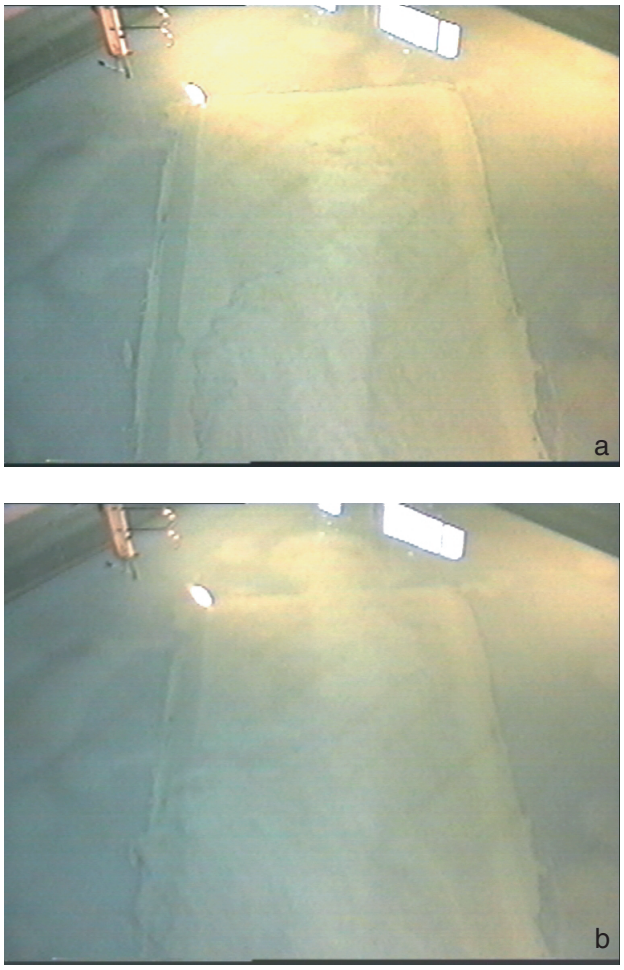

Figure 5: Experimental turbidity current traversing the channel.

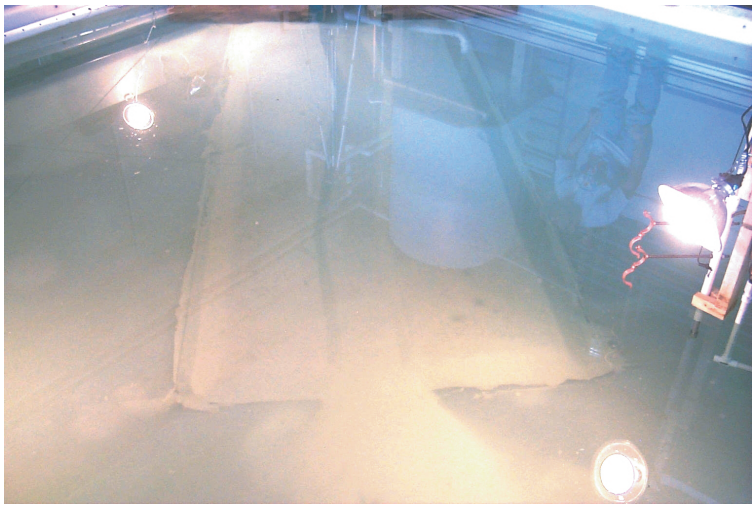

Figure 6: Experimental turbidity current lobe deposit.

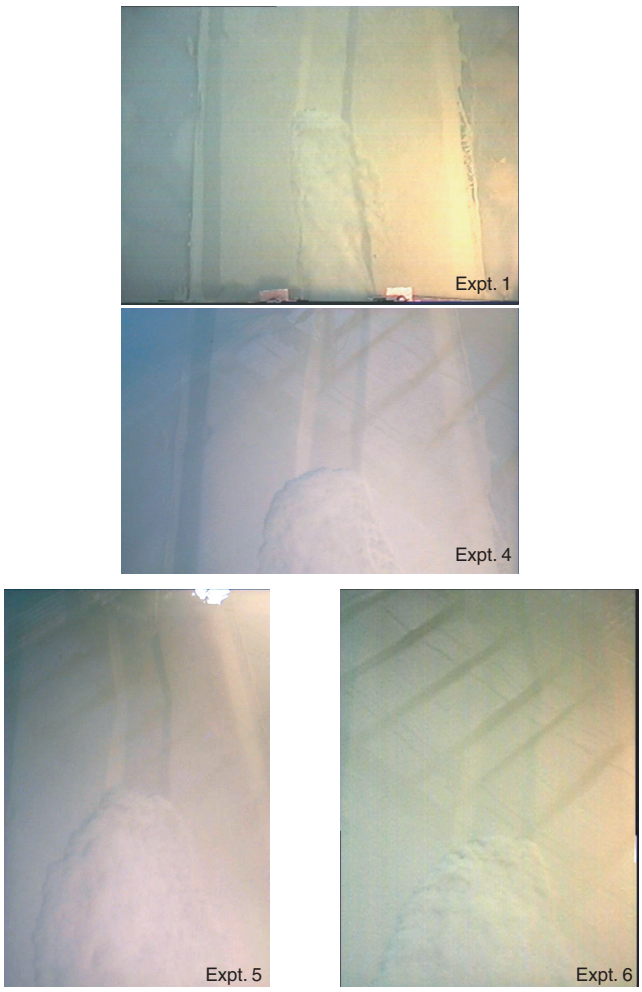

Figure 7: Turbidity current morphology in successive experiments.

iment 5 as the current fronts approach bend 2. Overall, the amount of sediment being overspilled in experiment 5 is much greater than that in experiment 4. In experiment 4, overspilling is asymmetric, predominantly occurring on the left bank. In contrast, overspilling in experiment 5 is symmetric relative to experiment 1, occurring on both the left and right banks. However, it is clear that left bank overspilling dominates right bank overspilling in both experiments. The conditions of experiment 5 indicate there would be an associated increase in the lateral and downstream extent of overbank deposits.

It should be noted that even for the case of strongest current confinement by the channel (e.g. experiment 1), the overspilling portion of the current never becomes detached from the main flow in the channel. In other words, for the low curvature or sinuosity of the present experimental channel, the current never experiences flow stripping. The current is best characterized by continuous overspilling modulated by the channel geometry.

3.3 Sediment Deposit Distribution

Figure 9 shows the processed acoustic image of the initial model channel configuration. Cross section locations discussed later in this section are marked. The filled circles are the locations at which aggradation rates were measured. Turbidity currents traverse the channel from right to left. The color bar shows the initial depth of the channel in cm. Depth increases from left to right on the scale. Initially, the channel has a slight variation in depth (increasing downstream) and a high spot on the left bank just beyond the crossing point. Sloping bank walls can be seen clearly (compare to Figure 2).

3.3.1 Spatial and Temporal Variations: Acoustic Maps

In the following figures, residual sediment thickness or aggradation maps, were constructed by taking the difference between the depth of the initial channel (Figure 9) and the depth of subsequent channels. These figures indicate increased or decreased deposition relative to the base channel. The color bar (in cm) indicates decrease in depth (thicker deposits) from left to right. Values to the left of (below) zero are negative. Negative values are most likely the result of the data smoothing process, rather than being a result of any net erosion. Three zones of deposition can be identified: a channel zone, an overbank zone, and a lobe zone.

Figure 10 shows the relative deposit thickness after the passage of the first turbidity current (experiment 1). In general, the deposit is thickest in the channel relative to the overbank or lobe zones. Channel deposits are thicker near the source and decrease downstream. Figure 11 shows the change in deposit thickness along the channel centerline. The channel has aggraded ~ 5 mm upstream of bend 1 and ~ 4 mm downstream of bend 2 (resid 01 in Figure 11). The deposit pattern indicates that, relative to the downstream end of the channel, a large amount of sediment drops out of the current in a region extending from the source to just past bend 1. Upstream to downstream thickness variations

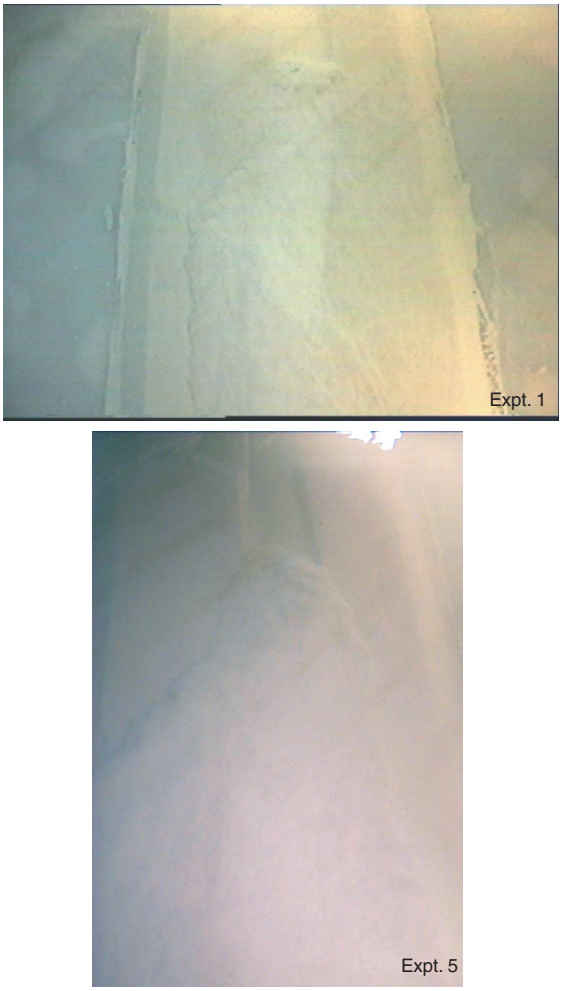

Figure 8: Overspill comparison of experiment 1 and experiment 5.

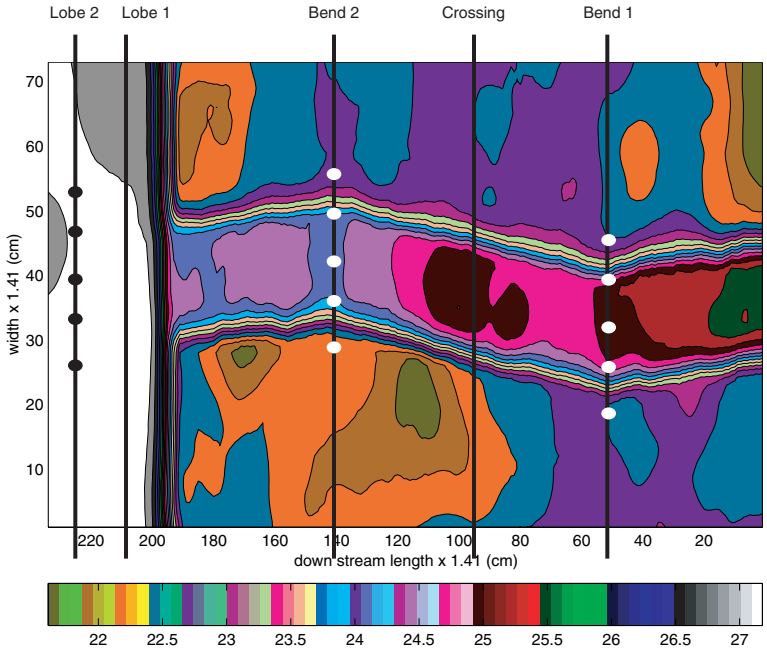

Figure 9: Initial channel configuration. Location of cross sections are shown. The filled circles are the ultrasonic probe sampling points used for calculation of deposition rates. Color bar in cm.

result from the loss of turbidity current energy as the current enters the channel. Preferential deposition also occurs along the right bank of the channel, extending past bend 2. This tendency will be explored further in subsequent figures.

Overbank deposits in Figure 10 are extensive, occurring on both the right and left banks near bend 1 and on the right bank of bend 2. Overbank deposits are generally very thin, but do show a lateral decrease in thickness from the channel bank outward. The deposits are on the order of 1 mm to 1.5 mm thick, and laterally thin changing by $\sim$ 1 mm over 30 cm. A thick overbank deposit accumulates just downstream of bend 1. Sediment thickness increases to $\sim$ 3 mm here. Deposits on the left bank are radially distributed away from and downstream of bend 1, reaching just upstream of bend 2.

Lobe deposits in Figure 10 are very thin, ranging from $\sim$ 1 - 3 mm thick. The thickest portion of the deposit is focused downstream of the left channel bank. It is apparent that the deposit is thickest in the center and falls off near its edges. The deposit has spread to a width of $\sim$ 25 cm.

Figure 12 shows the relative deposit thickness after the passage of the fourth turbidity current (experiment 4). Deposit thickness in the channel decreases downstream, but is primarily focused along the right bank beyond bend 1. The thicker portion of the deposit has migrated from bend 1 to just upstream of bend 2 (relative to Figure 10). Figure 11 (curve resid 04) shows that along the centerline the channel has aggraded to $\sim$ 2.2 cm upstream of bend 1 and $\sim$ 1.2 cm downstream of bend 2. The thickest point of the deposit occurs near the left bank upstream of bend 1.

The thickest overbank deposits occur on the left bank downstream of bend 1. The deposit has spread laterally and aggraded to a maximum thickness of $\sim$ 8 mm just over the left channel bank. The gradient from the bend corner is now $\sim$ 8mm $\rightarrow$ 2 mm over $\sim$ 20 cm. Overbank deposits continue to thicken and spread on the right bank upstream of bend 1. At bend 2, overbank deposits have thickened and spread radially, but are still much less developed than those outside of bend 1.

Lobe deposit thickness increased to a maximum depth of $\sim$ 6 mm. The primary locus of lobe deposition is shifted toward the channel center. The deposit is broader, covering a width of $\sim$ 38 cm, and the locus of maximum thickness is more defined relative to Figure 10.

Figure 13 shows the relative deposit thickness after the passage of the sixth turbidity current (experiment 6). Channel centerline thickness is shown in Figure 11 (resid 06). Channel aggradation upstream of bend 1 is $\sim$ 3.7 cm and $\sim$ 1.6 cm downstream of bend 2. Thick channel deposits downstream of bend 1 have migrated to the axis of bend 2 and are still focused along the right bank. Thicker deposits occur along the right bank because the geometry of bend 1 influences the front of the passing turbidity current. Figure 14 shows the current front geometry in experiments 1, 3, 4, and 5 just downstream of bend 1. As the current moves through the bend, the fluid velocity near the outer bend is higher than the fluid velocity near the inner bend. Asymmetry in the front velocity implies an asymmetry in the local buoyancy flux per unit width (Parsons et al.,

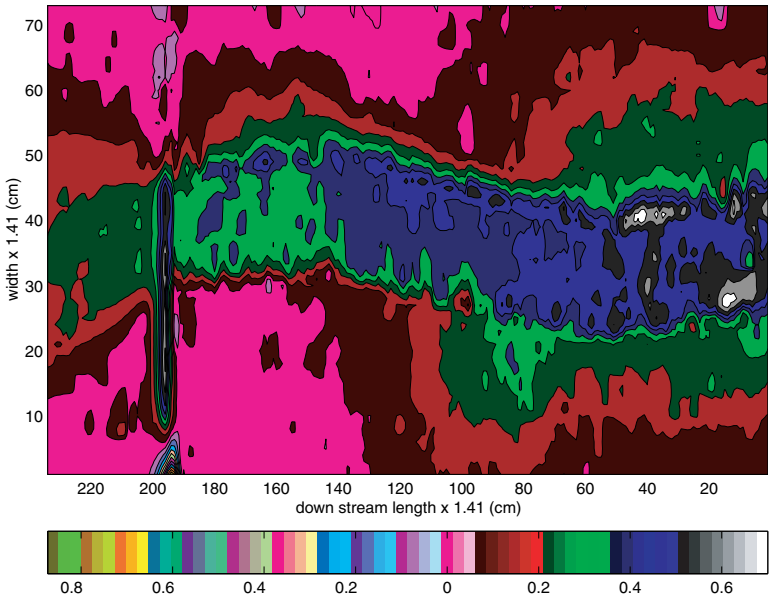

Figure 10: Difference in deposit thickness between the initial configuration and experiment 1, indicating increased or decreased deposition. Color bar in cm.

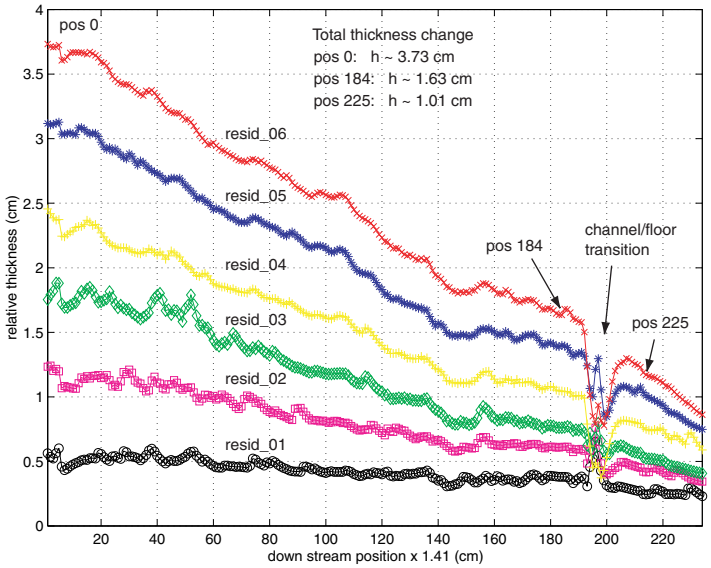

Figure 11: Change in channel centerline deposit thickness with time.

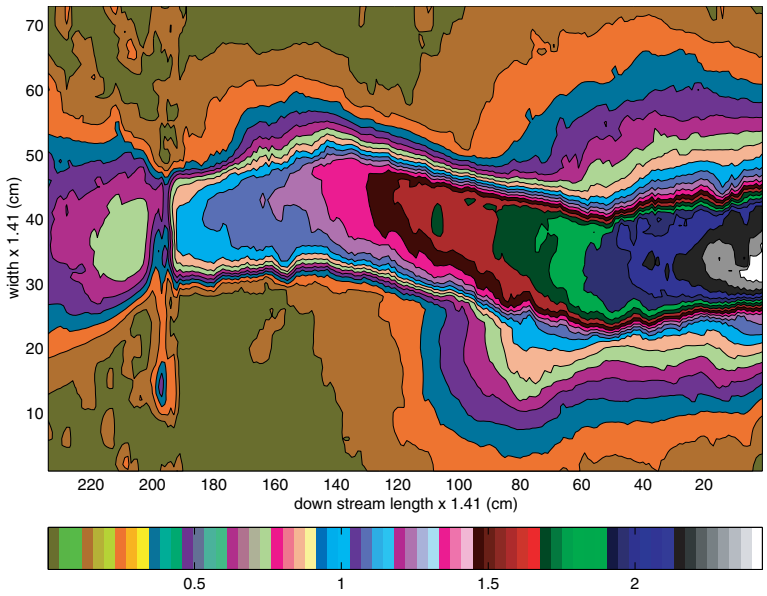

Figure 12: Difference in deposit thickness between the initial configuration and experiment 4, indicating increased or decreased deposition. Color bar in cm.

2001). This means that less (more) sediment is being transported along the right (left) bank in the straight channel segment. The left bank acts as a bypass zone relative to the right bank. This velocity asymmetry is present in all of the experiments (Figure 14).

As the current moves along the straight segment of the channel, the front velocity begins to smooth out, and the front shape begins to be more lobate (similar to the front shape before the current reached bend 1). However, the front velocity does not completely recover before it reaches bend 2. In other words, the front velocity of the current has a memory that lasts into bend 2. As the current passes through bend 2 the asymmetry of the front velocity switches, with the fluid velocity near the right bank increasing (outer bend of bend 2). The affect on the current front is less dramatic compared to that from bend 1. This is most likely due to the current moving into bend 2 with an initial velocity asymmetry (memory). Since the current velocity in the straight segment is slower along the right bank relative to the left bank, more sediment drops out of suspension there. Thicker deposits also occur along the left bank downstream of bend 2, although they are not as strongly focused as those in the straight channel segment.

Asymmetry of the front velocity is most likely due to the geometry of the channel since it is observed in all of the experiments. However, as mentioned above, geometrical friction may be important in controlling the front velocity distribution. The slope of the bank walls may also influence the flow field in the current. Superelevation of the fluid probably occurs along the outer bank of a bend (Imran et al., 1999). Current superelevation may be enhanced by the sloping wall, increasing the driving force on the fluid near the outer bend and resulting in an increase in fluid velocity. It should also be noted that the degree and extent of thicker deposits along any bank is probably controlled by the wavelength, bend curvature, and bend peak to peak amplitude. The experiments indicate that a long straight segment of channel between two bends will allow the turbidity current front to reestablish a more uniform velocity field. This observation suggests that a current's memory has a time scale that is related to the geometry of the channel.

Overbank deposits on both the right and left banks near bend 1 in Figure 13 have thickened and expanded. The deposit thickness on the left bank just downstream of bend 1 has increased to ~ 1.7 cm. This region of overbank deposit has not only expanded radially, but has also migrated downstream. The deposit along the left bank of the straight portion of the channel (channel crossing) has thickened due to the expansion and migration of the bend 1 overbank deposit. The deposit on the left bank is therefore thicker than the deposit on the right bank. The overbank deposit thickness has asymmetrically evolved across the straight section. These observations suggest that asymmetry in levee deposits along a channel segment may occur as a result of turbidity current overspill from an upstream bend.

Lobe deposit thickness decreases downstream of the channel exit (Figure 13). This is due to the thickness of the deposit approaching the relief of the channel. In subsequent experiments, the relief between the lobe and the channel bed is

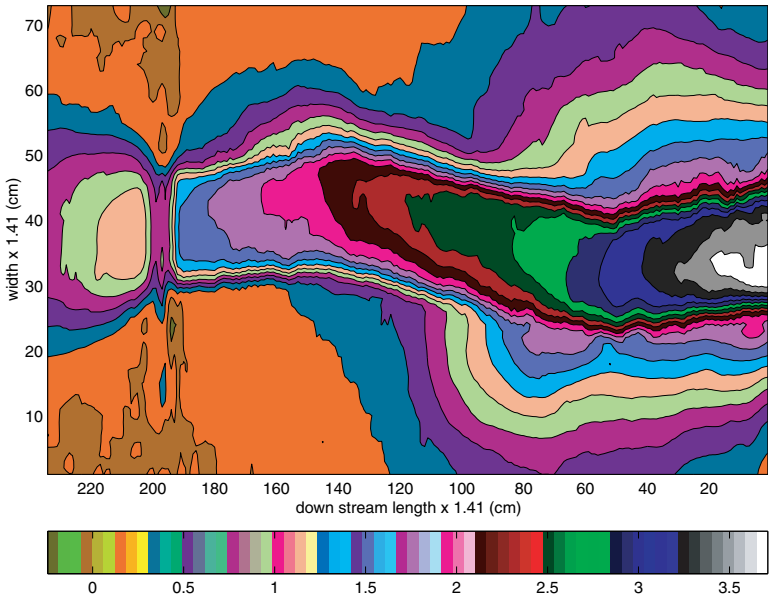

Figure 13: Difference in deposit thickness between the initial configuration and experiment 6, indicating increased or decreased deposition. Color bar in cm.

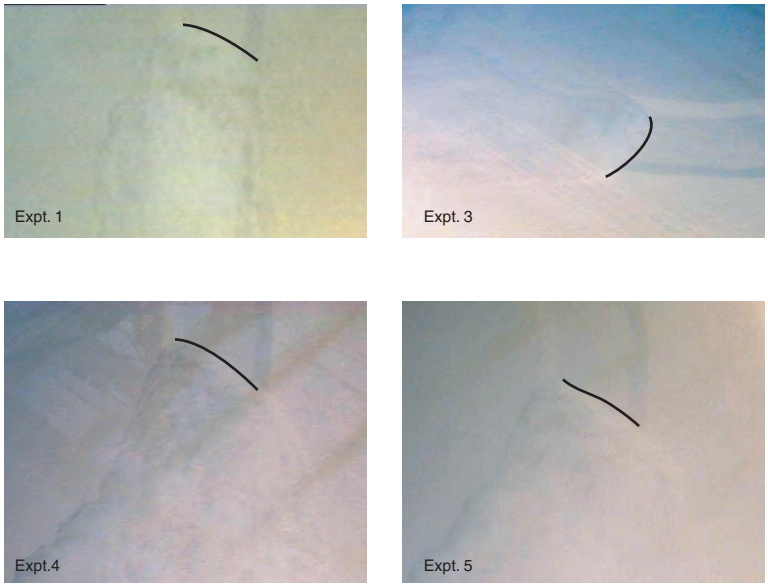

Figure 14: Geometry of the current front for different experiments. The non-uniform front velocity of the current is observed in all of the experiments. The black lines outline the shape of the current front.

reduced. Therefore, the current slows down closer to the channel exit, causing sediment to drop out of suspension. Lobe aggradation is $\sim$ 1 cm (Figure 11), and a spread of $\sim$ 40 cm in width.

3.3.2 Spatial and Temporal Variations: Cross Sections

Figures 15 - 19 show channel cross sections at bend 1, the channel crossing, bend 2, lobe 1, and lobe 2, respectively (refer to Figure 9 for locations). The downstream direction is into the page. The bottom curve is the initial channel geometry (experiment 0) and the top curve is experiment 6 (shallowest depth). Successive experiments are in between. Each figure represents a time slice of the deposit at that location. Note the large vertical exaggeration.

A cross section at bend 1 is shown in Figure 15. An examination of the initial geometry (Expt 0) shows that the right bank levee was initially shallower than the left bank levee by $\sim$ 1 mm, and that the outer bend channel floor was slightly shallower than the inner bend channel floor by $\sim$ 1 mm (slope of $\sim$ 0.006 or $\sim 0.3^o$).

As each turbidity current passes, the channel floor asymmetrically aggrades and the banks preferentially grow from the bank break outward. The bank break is the approximate location of the transition between the levee and the channel, and is defined by the change in slope of an elevation curve. The elevation curve of experiment 6 (see Figure 15) shows that the channel floor near the outer bend is $\sim$ 1.5 - 1.7 mm shallower than the floor near the inner bend. The slope of the floor is $\sim$ 0.0096 ($\sim 0.55^o$). The change in the magnitude of floor slope over the course of the experiments (S_6/S_0, S is slope and 6, 0 are experiment numbers) is 1.6. The bank slopes also decreased. The outer bank slope decreased from $\sim 16^o$ (initial configuration) to $\sim 6^o$ in experiment 6.

Thick levee deposits form at the bank break on both the left and right banks. The width of the thickest deposit on the left bank levee is less than that on the right bank levee. However, the slope of the left bank levee is $\sim$ 0.035 ($\sim 2.03^o$) and the right bank levee is $\sim$ 0.027 ($\sim 1.56^o$). This indicates that the interaction of the current with the outer bend may have significant influence on the amount and direction of the overbank sediment flux. The elevation difference between the right and left levee maximums is $\sim$ 1.3 mm. The elevation difference has changed by only 0.3 mm relative to the initial configuration.

Bend growth and/or migration is difficult to determine. Since the plotted data are smoothed, the location of the bank break through time cannot be determined precisely. The shape of the curves (their gull wing appearance) suggests that the bend may be moving to the left, indicating an increase in bend amplitude. Sectioning the deposit and/or conducting more experiments may help us determine whether the bend is growing/migrating.

In Figure 16 channel cross sections at the approximate mid-point between bend 1 and bend 2 are plotted. The initial channel geometry shows that the left bank levee is shallower than the right bank levee by $\sim$ 5.5 mm and that the right bank channel floor is shallower than the left bank channel floor by $\sim$ 0.6 mm (slope of $\sim$ 0.004, or $\sim 0.24^o$).

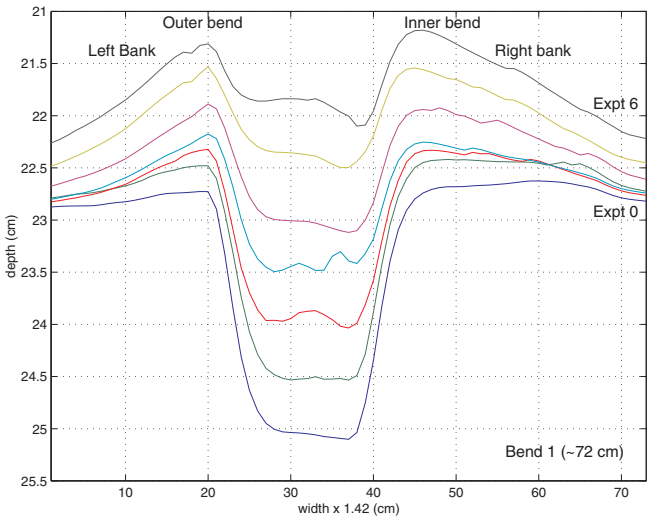

Figure 15: Channel cross section at bend 1.

In the elevation curve of experiment 6, the channel floor at the crossing asymmetrically aggrades, with preferred deposition near the right bank. The channel floor near the right bank is ~ 2.3 mm shallower than the floor near the left bank (compare to Figure 13). The floor slope is ~ 0.016 ($\sim 0.93^o$). The change in the magnitude of floor slope over the course of the experiments is $S_6/S_0 = 4.0$

Levee growth on the left bank is quite different than that on the right bank. The maximum deposit thickness on the left bank does not occur at the bank break but is displaced to the left by ~ 10 cm. Compare this to the maximum on the right bank levee that occurs at the right bank break. The shift in minimum elevation correlates with the shallow spot that was formed on the initial deposit (see the location of the high spot in Figure 9). Deposit thickness on the left bank is distributed uniformly about the maximum. In contrast, deposit thickness on the right bank levee falls off just to the right of the maximum. The total change in maximum elevation (relative to the initial configuration) of the left levee is greater than that of the right levee (~ 1.13 cm to ~ 0.81 cm, respectively). The dramatic asymmetry of the levee deposits is due to the influx of sediment that overspilled at bend 1 upstream of the channel crossing. The sediment influx most likely enhanced the normal sediment accumulation from localized overspill. This cross section also shows that an upstream bend can affect downstream levee morphology and deposition.

Figure 17 shows the channel cross section at bend 2. Initially, the left bank levee is shallower than the right bank levee by ~ 5.0 mm, and the left bank channel floor is shallower than the right bank channel floor by ~ 0.8 mm (slope of ~ 0.006, or $\sim 0.36^o$).

As in the above cross sections, the elevation curve of experiment 6 shows that the channel floor at bend 2 asymmetrically aggrades, with preferred deposition near the right bank. The channel floor near the right bank is ~ 0.5 mm shallower than the floor near the left bank (compare to Figure 13). The floor slope is ~ 0.004 ($\sim 0.23^o$). The change in the magnitude of floor slope over the course of the experiments is $S_6/S_0 = 0.67$. The slope ratio is less than one because the slope of the channel floor switches from shallow depth near the left bend to shallow depth near the right bend.

Maximum deposit thickness occurs at the bend break on both right and left levees. However, the total change in levee height (deposit thickness) on the right bank is greater than that on the left bank. The total elevation change on the right levee at the deposit maximum is ~ 1.01 cm, and ~ 3.3 mm at the deposit maximum on the left levee. The slope on the right levee flank is larger (~ 0.046, $\sim 2.6^o$) than that on the left levee flank (~ 0.02, $\sim 1.2^o$).

It is difficult to determine if the bend is growing. The shape of the curves suggest that the bend may be growing to the right, indicating an increase in bend amplitude. Again, sectioning the deposit and/or conducting more experiments may help us determine whether the bend is growing/migrating.

Figure 18 shows the lobe 1 deposit cross section located near the channel exit. The tank floor depth is the initial condition curve. The low spot in the middle is a floor seam that passes at an angle to the channel form. Deposit

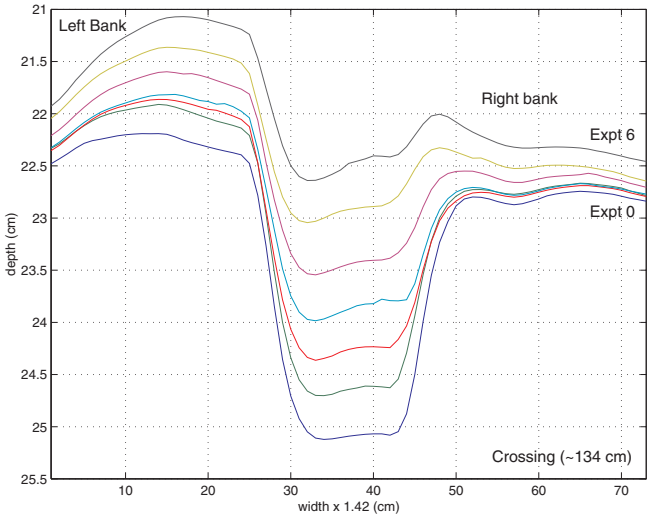

Figure 16: Channel cross section at the crossing between bend 1 and bend 2.

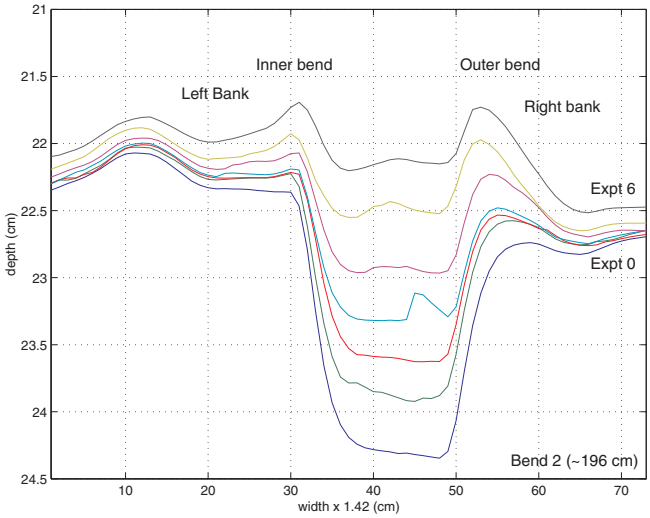

Figure 17: Channel cross section at bend 2.

thickness is asymmetric, being thicker on the left bank. The asymmetry may be due to the dynamics of the turbidity currents as they pass out of the channel. Current front velocity may be affected at bend 2 in a similar fashion to that at bend 1. A current may enter the lobe region with a slightly smaller front velocity near the left bank, resulting in an increase in sediment deposition on the left bank side (see discussion in section 3.3.1). The maximum deposit thickness is $\sim$ 1.3 cm.

Figure 19 shows the lobe 2 deposit cross section located downstream of lobe 1. The deposit is symmetric about the centerline. Deposit symmetry at this location may be due to spreading of the depositing turbidity current. By this point, the current front velocity has smoothed out, promoting uniform deposition (see Figure 5a). The maximum deposit thickness is $\sim$ 1.01 cm.

3.3.3 Deposition Rates

In an attempt to quantify grain size sorting trends and depositional asymmetry observed in the cross sections, we collected profiles of aggradation rate along a channel cross section during an experimental run (see Figure 9 for locations). We assume that aggradation rate, which is proportional to deposition rate (and grain settling velocity), is a function of grain size, with higher aggradation (deposition) rates corresponding to larger grain sizes dropping out of suspension. Over the course of an experimental run, the ultrasonic probe measured the change in deposit depth with time at pre-described points along a given profile. For the case of negligible erosion and bed load transport, aggradation rate is related to deposition rate by the generalized Exner equation

$$(1-\lambda)\frac{d\eta}{dt} = D$$

where D is deposition rate, λ is porosity, and $d\eta/dt$ is aggradation rate. We assume the above equation applies to the mean grain size of our sediment. In our experiments, $d\eta/dt$ is the slope of the curve of the change in bed elevation with time. Figure 20 shows the results using a porosity of 0.5 at cross sections bend 1, bend 2, and lobe 2. Each point shows the deposition rate at a given cross section and each curve shows the deposition rate trend as a function of downstream position.

Interpretations of cross-channel grain size sorting cannot be made because of measurement errors in the data. However, the fall-off of deposition rate in the downstream direction is probably representative of grain size sorting. Reduction in deposition rate is a result of either the reduction in the mean grain settling velocity (implying a reduction of mean grain sized in suspension) or a change in the current sediment concentration near the bed (Imran et al., 1998; Garcia, 1994). Because our currents are of short duration, the near bed sediment concentration probably does not change much during the course of an experiment, therefore a reduction in mean grain settling velocity probably controls the deposition rate. The trend of the curves suggests that grain size decreases

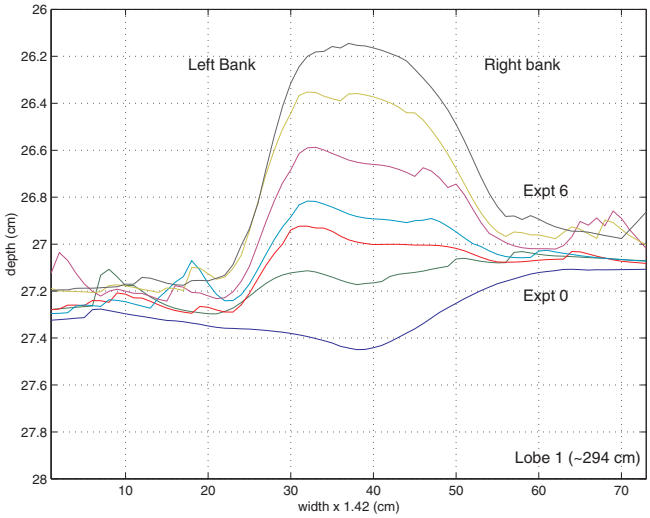

Figure 18: Lobe 1 deposit cross section.

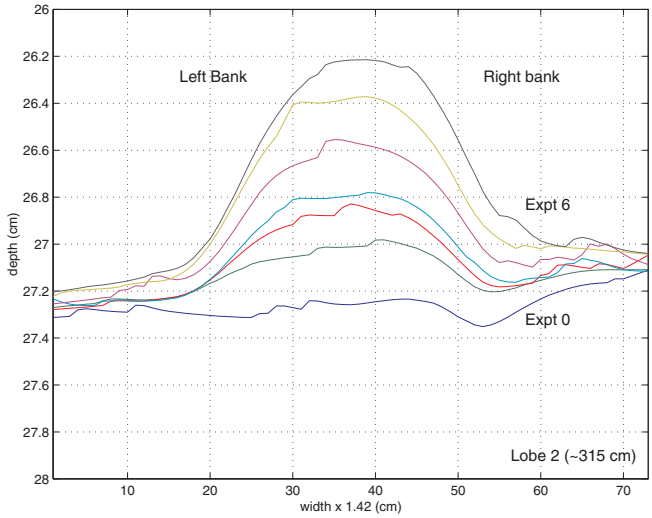

Figure 19: Lobe 2 deposit cross section.

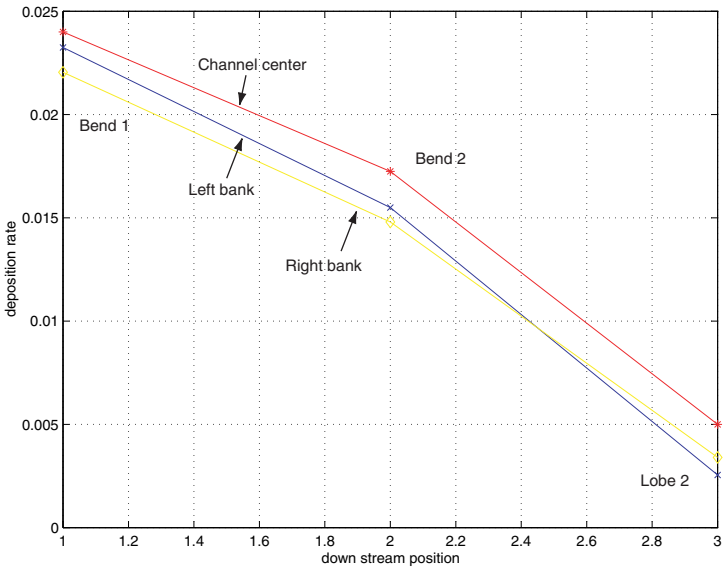

Figure 20: Deposition rate at downstream cross sections. Locations are marked (refer to Figure 9). Curve locations are relative to an observer looking downstream.

downstream, with the coarsest grains near bend 1 and the finest grains at the lobe. Sectioning of the deposit is needed to corroborate this interpretation.

4 Implications for Sandstone Deposits

Sequences in the experimental turbidite beds will be characterized by a combination of down-channel, cross-channel, and vertical variations in grain size. Grain size sorting in the deposit will be a result of the interaction of a turbidity current with the channel geometry. These sorting patterns may have implications for bed connectivity and correlation, and for the way their reservoir properties vary.

At present, the best way to construct down-channel, cross-channel, and vertical profiles of grain size distribution, sorting and channel evolution is to section and sample our final deposit. Unfortunately, by the writing of this paper, experiments are still being conducted. However, a glimpse of grain size sorting and channel evolution can be inferred from the ultrasonic probe data and video observations discussed in previous sections. Ultimately, we hope to use the acoustic data to characterize and interpret each deposit while using sectioning and sampling to ground truth the interpretations. In the current experimental setup, it is unclear how deposition upstream of bend 1 is influenced by proximity to the source. Therefore, only deposits located downstream of, and including bend 1, will be considered.

We will attempt to deduce the spatial patterns of grain size sorting by applying the net acceleration conceptual framework presented in Kneller (1995) (with similar caveats). This section is separated into three discussions: overbank deposits, channel deposits, and lobe deposits.

4.1 Overbank Deposits

Overbank deposits on the left bank of bend 1 are thickest near the bend break while thinning in a radial pattern away from the bend apex (see Figure 13). Overbank deposits on the right bank of bend 2 are thickest near the bend break while thinning in a weak radial pattern away from the bend apex (see Figure 13). These deposits are built up from overspill of the upper dilute part of the turbidity currents. Since the finer components of the grain size distribution make up this portion of the current, these overbank deposits should contain the finest grain sizes along the entire channel system.

Grain size sorting in these deposits is probably controlled by a combination of channel aggradation and levee construction (see Figures 15 and 17). Over time, the slopes of the outer bend levee flanks increase, resulting in a condition of divergent or depletive flow of the overspilling sediment. In this case, the overspilling fluid should experience waning depletive conditions (Kneller, 1995) and develop a normally graded deposit that becomes thinner and finer-grained away from the bend break. However, as the channel aggrades, lower levels of the turbidity currents are elevated to the bend break, exposing coarser grained

sediment to overspill. This suggests that the mean grain size in successive deposits should increase.

4.2 Channel Deposits

Generally, channel deposits are thickest at bend 1 and thin downstream (see Figure 11). However, the deposit shows cross-channel asymmetry beyond bend 1. The thicker part of the deposit is near the right bank in the straight channel segment, near the outer bend at bend 2, and near the left bank beyond bend 2 (Figure 13). The sediments of these deposits are derived from the confined portion of the turbidity currents. Since the current dynamics are influenced by the channel geometry (see section 3.2.1), spatial variations in grain size will be complex.

Since downstream channel aggradation is not uniform, thicker deposits accumulate near bend 1 (see Figure 11). In this case, the experimental currents experience waning depletive conditions, resulting in a deposit that should be normally graded, and becomes thinner and finer-grained downstream. Figure 20 indicates that these types of deposits should occur. However, the influence of the channel geometry on the turbidity current flow dynamics (see Figure 14) should modify this simple picture. Cross-channel variations in grain size should be reflected in the deposit.

If we assume the variability in the current flow velocity (while in the straight channel segment between bend 1 and bend 2) is symmetric about the channel centerline, the left side of the flow will decelerate and the right side of the flow will accelerate as the current tries to re-equilibrate. In this case, the current on the left side will experience waning depletive conditions and the current on the right side will experience waxing depletive conditions. The deposits near the left bank should be normally graded, becoming thinner and finer-grained downstream. The deposits near the right bank should show coarsening upward beds which become finer-grained downstream. These conditions will be opposite downstream of bend 2. As previously mentioned (section 3.3.1), the degree and pattern of downstream grain size sorting will be a function of channel wavelength, bend curvature, and bend peak-to-peak amplitude. It should be noted that a decrease in channel levee relief in the downstream direction could change these conclusions.

The preceding analysis may also apply to the bend deposits if we neglect the effect of cross-channel currents on the deposits. Currents speed up along the outer bend relative to the inner bend. If the current traverse through the bend is long enough, the deposits near the inner bend should be normally graded, becoming thinner and finer-grained downstream. The deposits near the outer bend should show coarsening upward beds which become finer-grained downstream.

4.3 Lobe Deposits

The lobe deposit is thickest near the channel exit, thinning both downstream and laterally. The deposit has a lobate shape in both plan view, and is mounded

in cross section. Initially, the relief of the channel exit sets up a local flow non-uniformity, causing sediment to rapidly drop out of suspension.

Generally, the grain sizes of the lobe deposit will be smaller than those found upstream in the channel as mentioned in section 4.2, and as inferred in Figure 20. The exiting currents experience waning depletive conditions, resulting in a lobe deposit that should be normally graded, becoming thinner and finer-grained downstream. Also, since the current is no longer confined and can spread laterally, the deposit cross section should be normally graded, becoming thinner and finer-grained away from the lobe center. The coarsest grains should occur in the center of the lobe deposit close to the channel exit.

5 Summary and Conclusions

We have demonstrated that our experimental facility, data collection, and data processing system can give us a unique understanding of the processes and deposits that build submarine fan environments. We can construct submarine fan elements, generate scaled turbidity currents, collect three dimensional current velocity data, and determine bed thickness variations on the order of 100μ to 500μ. Our system collects and saves reflection waveforms from many points on each deposit, allowing a coherent analysis of deposit development in space and time. The waveforms also contain information that can be exploited in the future (e.g. examining the waveform offsets to determine lateral sorting patterns, proposed by Felix Herrmann of the Earth Resources Laboratory). The accessibility of the facility also allows us to ground truth the acoustic data by extensively sectioning the deposit.

Our preliminary results are qualitative, but indicate that channel wavelength, bend curvature, and bend peak to peak amplitude may have strong controls on down-channel and cross-channel depositional patterns, deposit thickness and grain size sorting. Our data show the construction of prominent levees, asymmetric levee growth (application to levee flank waves), continuous channel overspill, enhanced channel overspill downstream of bend corners, and lobate shaped lobe deposits.

Acknowledgments

Financial support for this research was provided by Chevron Petroleum Technology Corporation. This support is gratefully acknowledged. Thanks are due to Jeff Snyder for setting up the wiring of the servo motors and their controllers, Bill Lyons, who assisted in the experiments and has made many insightful comments about the results, and Jeff Parsons for his initial setup and introduction of the experiment.

References

M.H. Garcia. Depositional turbidity currents laden with poorly sorted sediment. *J. Hydr. Eng.*, 120(11), 1994.

M.H. Garcia and J.D. Parsons. Mixing at the front of gravity currents. *Dynamics of Atmos. and Oceans*, 24:197, 1996.

J. Imran, G. Parker, and N. Katopodes. A numerical model of channel inception on submarine fans. *Jour. of Geophysical Res.*, 103:1219, 1998.

J. Imran, G. Parker, and C. Pirmez. A nonlinear model of flow in meandering submarine and subaerial channels. *J. Fluid Mech.*, 400:295, 1999.

B. Kneller. Beyond the turbidite paradigm: physical models for deposition of turbidites and their implications for reservoir prediction. *From Hartley, A.J. and Prosser, D.J. (Eds.), Characterization of Deep Marine Clastic Systems, Geological Society Special Publication*, (94):31, 1995.

P.L. Manley, C. Pirmez, W. Busch, and A. Cramp. Grain-size characterization of amazon fand deposits and comparison to seismic facies units. *In: Flood, R.D., Piper, D.J.W., Klaus, A. Peterson, L.C. (Eds.), Proceedings of the Ocean Drilling Program, Scientific Results*, 155, 1997.

C.M.G. McHugh and W.B.F. Ryan. Sedimentary features associated with channel overbank flow: examples from the monterey fan. *Marine Geology*, 163: 199, 2000.

E. Mutti and W.R. Normark. *An intergrated approach to the study of turbidite systems*. In: Weimer, P., Link, M.H. (Eds.), Seismic Faces and Sedimentary Processes of Submarine Fans and Turbidite Systems (Frontiers in Sed. Geol.). Springer, New York, 1991.

W.R. Normark, H. Posamentier, and E. Mutti. Turbidite systems: state of the art and future directions. *Rev. Geophys.*, 31:91, 1993.

J.D. Parsons, W.J. Schweller, C.W. Stelting, J.B. Southard, W.J. Lyons, and J.P. Grotzinger. An experimental study of turbidite fan deposits. *Submitted Journal of Sedimentary Research*, 2001.

J. Peakall, B. McCaffrey, and B. Kneller. A process model for the evolution, morphology, and architecture of sinous submarine channels. *J. of Sed. Res.*, 70:434, 2000.